3-5 Development of Airborne high-resolution multi-parameter imaging radar SAR, Pi-SAR

UMEHARA Toshihiko, URATSUKA Seiho, KOBAYASHI Tatsuharu, SATAKE Makoto, NADAI Akitsugu, MAENO Hideo, MASUKO Harunobu, and SHIMADA Masanobu

The airborne X/L-band Synthetic Aperture Radar system (Polarimetric and Interferometric SAR, Pi-SAR) was developed by the Communications Research Laboratory and National Space Development Agency of Japan in their joint project from 1993 to 1996. The resolution of the X-band image is about 1.5 m and L-band is about 3.0m. Both SARs can make fully polarimetric observations. The X-band SAR has a cross-track interferometric function that measures the ground height with accuracy of 2 m. These systems are installed in the airplane, Gulfstream II. In this paper we describe our Pi-SAR system and the ground processing system. In addition, we also discuss the performance of our system by using the Pi-SAR datad.

Keywords
Synthetic Aperture Radar(SAR), High-resolution, Polarimetry, Interferometry, Dual frequency

1 Introduction

In recent years, the global environment issues have been drawing greater attention worldwide. In this context, remote sensing technology is expected to contribute to the monitoring of desertification and observations of volcanic eruptions, earthquakes, and forest fires. Radio waves are useful in such observations in that they are not affected by weather conditions and in that they allow observation on a 24-hour basis. Synthetic aperture radar (SAR), one type of microwave remote sensor, transmits microwaves from an airplane or a satellite, receives the echoes returned from the ground surface. This radar system can attain significantly high resolution through the use of advanced signal processing such as aperture synthesizing and pulse compression. The images provided by SAR appear quite similar to monochrome aircraft photograph. Moreover, the SAR's use of microwaves has the advantage of rendering it capable of acquiring images at any time of day or night, and even under adverse conditions like cloud covers. In addition, SAR can identify objects in a manner different from that of optical sensors, as light and microwaves show different behaviors in scattering and reflection. SAR has already been mounted on satellites and used in military applications. When mounted on an airplane, SAR provides diverse observation opportunities where parameters such as resolution, observation range, and incident angle are optimized for each observation purpose. Although observation width becomes narrow, an airborne SAR can obtain a high-resolution image with 10 times the resolution as this image taken from a satellite-borne SAR.

Further, improved hardware will make cutting-edge observation functions available for application experiments. While a satellite-borne radar system acquires observation data once following virtually the same flight course and direction, airplane-borne SAR can perform quick observations in arbitrary directions

and, in the event of a disaster, for example, it can provide observations every day or multiple times in one day.

Since 1993 the Communications Research Laboratory and the National Space Development Agency of Japan have been jointly developing an airborne three-dimensional high-resolution X- and L-band imaging radar (Pi-SAR: Polarimetric and Interferometric SAR) and carrying out a number of related experiments. Designed not only for experimental purposes but also for practical use, this radar system is installed in a small jet and is capable of measuring the ground surface under the left side of the plane at a width of up to 40 km, from an altitude of approximately 40,000 feet (12,000 m). Pi-SAR is a multifunctional, high-performance radar system, featuring innovative interferometric and polarimetric observation functions. This paper describes the Pi-SAR system, its data processing system and data processing steps, and provides an evaluation of its capabilities based on the obtained observation results.

2 Principles of Imaging Radar and Synthetic Aperture Radar

2.1 Microwave Imaging Radar

Microwave imaging radar transmits radio pulses downward and slantly in a direction, normal to the advancing direction of an aircraft or satellite, and receives the echoes returned from the ground as shown in Fig.1. Since the time a pulse takes to return home is proportional to the distance to the ground, the received pulses provide a scattering profile of the ground perpendicular to the advancing direction of the radar. As the radar proceeds in the azimuth direction, it provides two-dimensional ground images. The image resolution in the range direction is determined by the pulse width of the radar, while the azimuth resolution is determined by the antenna beam width in the azimuth direction. In general, the imaging radar adopts an antenna with a "fan beam" type pattern that is very sharp in the azimuth direction and relatively wide in the cross-track direction either to the left or right side of the advancing direction. If the pulse width is narrowed, the resolution in the range direction is increased, but the S/N (signal-to-noise) ratio declines as the transmission power becomes low. Meanwhile, since the azimuth resolution is determined by the beam width, the beam width spreads in proportion to the flight height and the resolution declines accordingly. In order to maintain resolution levels in flights at high altitudes, the beam should be narrowed in the azimuth direction; thus, a large antenna will be required. Indeed, one imaging radar we previously developed featured an antenna aperture of about 3.5 m [1], so as to maintain a resolution of about 60 m at an altitude of 3,000 m at an incidence angle of 60 degrees.

In contrast to this approach, movement in the azimuth direction can be used to synthesize an equivalent array antenna in a technique called "synthetic aperture radar (SAR)" as described next.

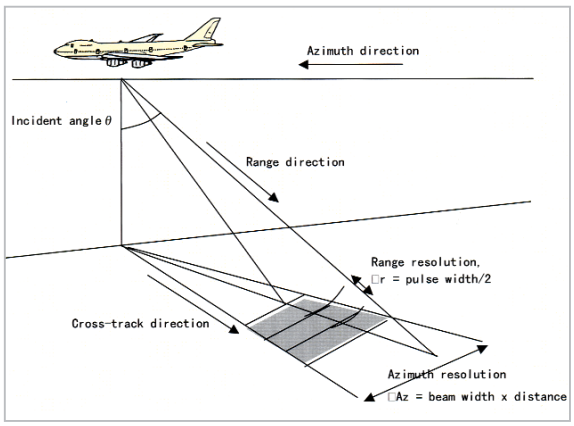

Fig.1 *Principle of microwave imaging radar*

2.2 Synthetic Aperture Radar (SAR)

When focusing on a single target, for example, with moving radar having a relatively broad beam in the azimuth direction, a target continues to receive the beam for the entire period during which the plane flies from position 1 to position 3, as shown in Fig.2. In other words, this is equivalent to using an antenna with an aperture substantially as large as L, or using an array antenna whose elements are extended from positions 1 to 3

along the flight course to receive the returned signals.

By synthesizing the signals received from such a "virtual" array antenna, the azimuth resolution can be narrowed down to half the real antenna aperture, regardless of flight altitude. Namely, if the S/N ratio is not taken into account, we can say that the smaller the antenna, the higher the resolution. On the other hand, pulse-compression technology is adopted to raise the range resolution. Specifically, FM chirp compression is usually adopted in SAR. FM chirp compression is a technique by which FM-modulated long pulses are transmitted and received by a matched filter with inverted frequency-delay characteristics to convert the original pulses into narrow ones of a larger power (Fig.3). Looking at this sort of aperture synthesis in a different way, it may be seen as a signal-processing method that uses an appropriate matched filter to capitalize on the fact that the Doppler effect (caused by the plane's movement against the ground) provides the same phase change as that resulting from FM modulation. In this sense, the process of aperture synthesis is referred to as azimuth compression.

For such range compression and azimuth compression, we must acquire signal waveform data, including phase information as well as signal intensity, using a receiver. As a result, the radar system becomes quite complex, relative to real aperture radar, and the required recording and processing data increases significantly in size. At the same time, the system features excellent resolution and a new function enabling the utilization of phase information. In short, the capabilities of interferometric and polarimetric observations create a distinctive advantage when performing observations of the ground surface[2][3].

(1) Interferometry

When two antennas are installed in the cross-track direction, as shown in Fig.4, the phase difference between signals captured by the two antennas is determined by the difference in distance from each antenna to the target, although this difference includes instabili-

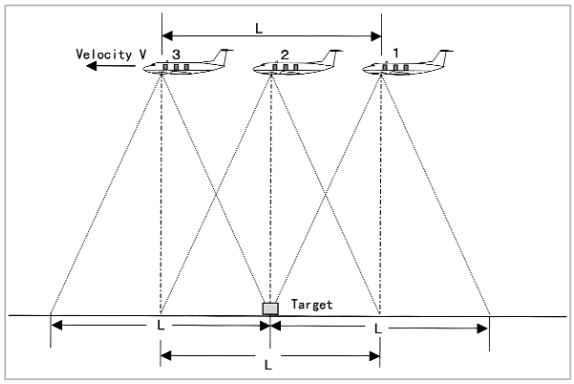

Fig.2 *Basic concept of azimuth compression*

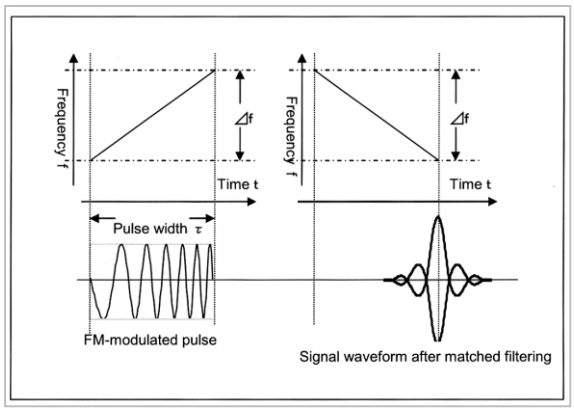

Fig.3 *Basic concept of chirp compression*

ty in integral multiples of 2π. Therefore, if the phase difference between the signals received by the two antennas is measured with high precision, Equation (1) provides the incidence angle, θ, at each point on the ground, while Equation (2) provides h[4].

$$\phi = \frac{2\pi}{\lambda} B \sin(\theta - \alpha) \quad (1)$$

$$h = H - R\cos\theta \quad (2)$$

where λ is wavelength, B is the baseline length between two antennas, α is the angle made between the baseline and horizontal line, H is the altitude of the platform, and R is the range distance.

(2) Polarimetry

Polarization is the trajectory of the electric field vector, a trajectory that changes along with time at different points in space. Usually such polarization is elliptical, but in some cases it may be circular or linear. If each of the transmitter and receiver antennas of the radar has the function of transmission and

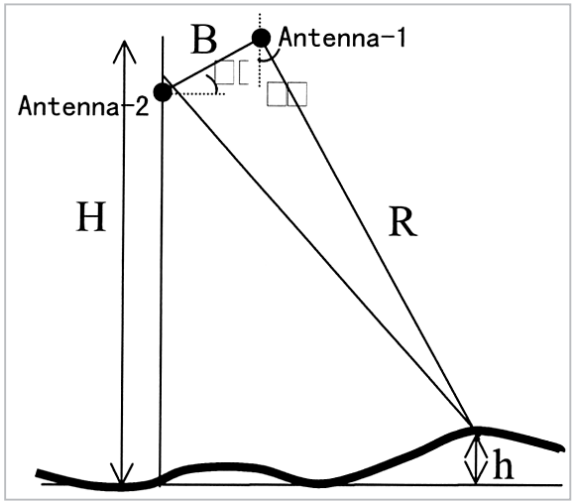

Fig.4 *Schematic description of height measurement (Inferometry)*

reception both horizontally and vertically polarized orthogonal waves almost simultaneously, a scattering matrix is provided that has four components combining the two (vertical and horizontal) polarization components in both transmission and reception. When the scattering matrix is made of complex numbers carrying the phase-relation information, the scattering (in elliptical polarization) from a target irradiated by polarized waves can be calculated by integrating those polarization components. In other words, all of the information related to polarimetry, including the backscattering coefficient, can be determined from the relations between these components, as each features a complex amplitude, although the scattering matrix features only four-fold information. This is an essential feature of polarimetry.

3 Pi-SAR System

Airborne three-dimensional high-resolution imaging radar (Pi-SAR) is a radar system developed jointly by the Communications Research Laboratory and the National Space Development Agency of Japan; this system enables observation of the ground surface

Table 1 *System parameter and performance*

	X-band SAR			L-band SAR	
Center Frequency	9.55 GHz			1.27GHz	
Peak Power	6.3kW			3.0kW	
Bandwidth	100MHz			50MHz	
Antenna(L×W)	1.05m × 0.19m			1.55m×0.65m	
Incidence Angle	10 to 75 degrees variable			20 to 60 degrees fix	
Observation Modes	2CH Polarimetry or Interferometry	4CH Polarimetry	6CH Polarimetry and Interferometry	1CH	4CH Polarimetry
Swath Width(slant) (speed : 220m/s)	20.6/42.9 km	9.4/20.4 km	5.6/12.9 km	42.9 km	20.4 km
Range Resolution	1.5/3 m	1.5/3 m	1.5/3 m	3/5/10/20m	3/5/10/20m
Azimuth Resolution (4-look Processing)	1.5/3m			3/6 m	
Interferometry Baseline Accuracy in height	Cross-track 2.3 m less than 2m (rms.)				
Sampling frequency	123.45/61.725 MHz			61.7/30.9 MHz	
Quantization bits	8 bits for both I and Q			8 bits for both I and Q	
Platform	Gulfstream II				

using dual frequencies simultaneously—the X-band (with a wavelength of 3.14 cm) and the L-band (with a wavelength of 23.6 cm). The horizontal resolution is 1.5 m in the X-band and 3 m in the L-band, and Pi-SAR is capable of polarimetric observations (by transmitting/receiving horizontally and vertically polarized waves) using either band. Pi-SAR also features an interferometric function to provide elevation profiles of the ground using two antennas through X-band observation. Table 1 shows the major specifications of Pi-SAR[5]. As shown in the block diagram in Fig.5, the transmission signals (100 MHz in the X-band or 50 MHz in the L-band) are fed to the antenna in the form of chirp signals and then irradiated to the ground. The radio waves reflected off of the ground are received by the antennas and subjected to A/D conversion in the receiver (with phase information maintained), after appropriate adjustment of receiver gain and other parameters. This data is saved in a data recorder along with supplemental data, including airplane attitude. The data recorded in tape media is instantaneously read out by a reading-head and then sent to a real-time processor. The real-time processor carries out necessary processing on the X- and L-band polarization data and visualizes the obtained image on a screen.

The system for the L-band can be described with almost the same block diagram as that for the X-band, except that it has no sub-antenna and only one data recorder. These systems are deployed together on a two-engine jet, the GulfStreamII. This airplane allows observation at high altitudes (typically 12,000 m) and at speeds of 220 m/s during observation[6].

3.1 Antenna Subsystem

For the polarimetric function, the X-band main-antenna is equipped to deal with both vertical and horizontal polarized waves. The sub-antenna, which is required for interferometry, employs vertically polarized waves, as the return power of these waves is relatively large. As indicated by Equation (4), the phase change grows in proportion to the distance (the length of baseline) between the main and sub antennas and the measurement accuracy in the ground height is improved accordingly. The two antennas should be firmly installed as far apart as possible, as fluctuations in the antenna position caused by airplane vibration result in measurement errors. When these were installed as shown in Fig.6, antenna separation was 2.3 m in this Pi-SAR configuration. Considering the gain and redome size, we determined the antenna dimensions as 19

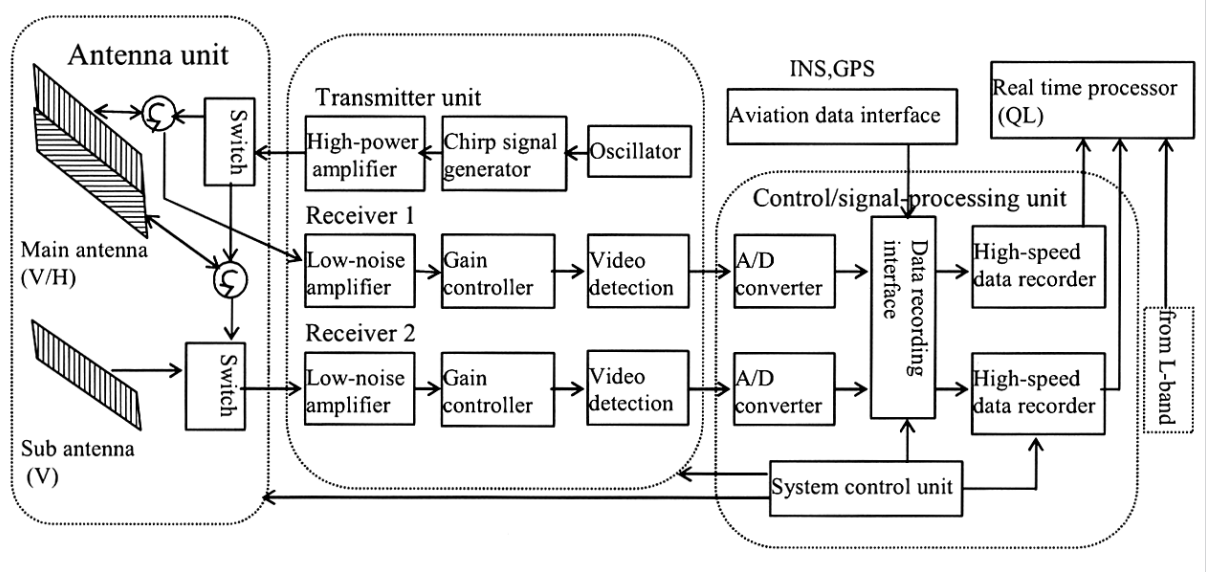

Fig.5 *Block diagram of X-band radar*

cm (6λ) in the vertical direction and 105 cm (30λ) in the horizontal direction. The width of the pencil-like beam in the azimuth direction was about 2.5 degrees. Furthermore, we formed a square-cosecant type fan-beam eliminating the change in received power so that the received power became almost constant, regardless of distance to the target in the elevation direction. To be specific, the received power fell within the -10 dB range over approximately 40 degrees. The antenna had a structure consisting of eight sub-array elements arranged at intervals of 1/2 across the center so as to provide phase coherence on the radiation device during the 100-MHz sweep. The roll angle was variable between 40 and 65 degrees (peak to peak) to extend the range of incidence angle selectivity for all target objects and observation modes. The dual-axis variable angle (within ±6.5 degrees) mechanism controlled the yaw angle so that the antennas were kept parallel to the traveling direction, regardless of the drift angle of the airplane.

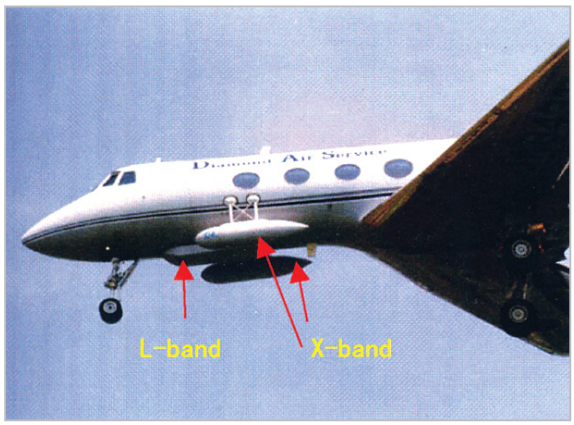

Fig.6 *An airplane instal led SAR*

Since L-band waves are longer in wavelength than X-band waves, the antenna must be larger. We adopted a micro-strip antenna that enabled transmission and reception of both horizontal and vertical polarization waves with a single antenna. The patch element was square so as to cut off the cross-polar component of the linear orthogonal vertical/horizontal polarization waves. The mounting unit for the antenna elements and feeder on the panel had a multi-layered structure adopting a dielectric honeycomb material to provide a lightweight, highly rigid antenna sub-panel. The antenna tilt angle in the elevation direction was 38 degrees so as to maintain power within the 10-dB range over about 40 (22 to 58) degrees. Fig.6 shows the external view of the antennas installed underside of the airplane.

The redome had a sandwich structure made of glass fabrics and epoxy resin, which materials are transparent to radio waves. The signal attenuation caused by the redome was around 0.1 dB. The redome for the X-band system was 45 cm in diameter, where the minor-axis aperture diameters of the vertical and horizontal antennas were 20 cm and the yaw angle was variable. The L-band system was mounted directly on the body of the airplane in order to reduce air resistance.

3.2 Transmitter Subsystem

An oscillator having a basic frequency of 12.34 MHz provides eight frequencies to be used inside the transmitter. A reference signal is created with a highly stabilized quartz oscillator using a quartz crystal under controlled temperatures for optimally stabilized operation; indeed, a frequency stability of 10^{-10} rms/sec is ensured for a short term. A chirp signal is created in the chirp generator by reading out (with the reference trigger) the waveform data saved in EPROM (12 bit digital data). Then, this is added to intermediate frequency and transferred to the radio frequency (either 9.55 GHz or 1.27 GHz).

The high-output amplifier for the X-band is made of a traveling wave tube (TWT) so as to maintain stability and reduce frequency-dependent fluctuations in the output level. This amplifier can provide an output power of about 6 kW at the antenna end. Meanwhile, a transistor-type high-power amplifier provides an output of 3 kW for the L-band. The amplified signal is supplied to either vertical or horizontal polarization antenna. Part of the amplified signal, branched with a coupler, is used to monitor transmission power and to

correct fluctuation.

In addition to independent observation, it is possible to use the L-band to determine which transmission and reception timings are synchronized with the reference frequency provided by the X-band system. Low-resolution (10 m and 20 m) modes are also available for simulation of the synthetic aperture radar system (ALOS/PALSAR) that will be mounted on a satellite scheduled to be launched in 2004.

3.3 Receiver Subsystem

The receiver system has two channels (1 and 2) of the same structure so as to receive vertical waves and horizontal waves at the same time and to enable it to handle two polarized waves separately, to perform the polarimetric function both in the X and L bands. In short, Channel 1 handles the vertical polarization signal, while Channel 2 handles the horizontal polarization signal. However, in order to perform interferometry and polarimetry at the same time in X-band observation, Channel 1 features a mode in which it switches the horizontally polarized wave of the main antenna and the vertically polarized wave of the sub-antenna alternately for each pulse, as well as another mode in which it handles only the sub-antenna signals for interferometry alone. When this mode adopted by Channel 1, Channel 2 handles only the vertically polarized wave of the primary antenna.

Received signals in the two channels pass a limiter and a bandpass filter and then enter the first stage low-noise amplifier—a FET amplifier capable of reducing the noise level to 3 dB or lower. After a frequency conversion in the gain control unit, the signals pass sensitive time control (STC) and auto gain control (AGC) units. Finally, the signals are divided into two components, (I,Q), having phase angles 90 degrees apart and detected as such so that complex signals having phase information can be obtained. Each of these signal components is passed through an A/D converter to become digital data.

3.4 Control and Signal Processing Unit

This system aims to identify the target objects based on phase information. Thus all the signal processing units are required to work in synchronization. For this purpose, all the hardware is controlled by the reference signal provided by the frequency generator. Further, X-band and L-band observations are synchronized by supplying the X-side 1-MHz and 123-MHz clocks to the L-side.

Airplanes are subject to attitude fluctuations of shorter intervals than those of satellites. The synthetic aperture radar mounted on an aircraft, therefore, requires as much real-time aircraft attitude data as possible. For this purpose, our system is equipped with high-precision sensor systems such as an inertial navigation system (INS) and a GPS to provide information about position and attitude. This information is collected by the signal-processing unit and saved in a data recorder along with I and Q data obtained by the receiver.

One of the benefits of the synthetic aperture radar lies in its generation of large quantities of data. Approximately three minutes of s in a flight of experiment produces about 12 GB of X-band data and 6 GB of L-band data. For data storage, we have adopted two high-speed data recorders (DIR-1000) for X-band data storage and one DIR-1000 for L-band data storage. The data transmission rate of this type recorder is 256 Mbps per unit. Each cassette has a large data capacity of 90 GB per cassette; however, this is used within about 50 minutes of continuous observation.

3.5 Real Time Processor

The airborne SAR is distinguished by its rapid availability in the event of a disaster, and can be used to gather information on a real-time basis during a disaster. To meet the requirements related to such applications, a real time processor was installed in the SAR in 2000. This device can reproduce and process arbitrary X- and L-band polarimetric data acquired in observation to provide an initial overview. The number of data acquisition points, however, is fixed at 1,024 in the range

direction, due to limitations of data size and processing rate, and its bandwidth changes with resolution (max. 2.5 m). Table 2 lists the parameter settings, selectable via a switch. When reading out the data written on the tape in the recorder and transferring the readout data to the real time processor, it is possible to check to determine whether or not the written data is correct. The processed image data is displayed on-screen, and image data for each page can be saved to a magneto-optical (MO) disk.

Table 2 *Selective parameters for real time processing*

Input data	Resolution	Process area (Range)
X1-VV	2.5m (X)	2.56km
X1-HV	5m (X,L)	5.12km
X1-VM	10m (X,L)	10.24km
X2-VH	20m (X,L)	20.48km
X2-HH		
X2-VS		
L-VV		
L-VH		
L-HV		
L-HH		

4 Observation Plan and Operation

4.1 Observation Plan

The airborne SAR measures the area under the plane on its left side in a slanted direction with a fixed width. We must determine the flight course in advance to most efficiently cover the target areas. For this purpose, the latitude and longitude information for the target areas must be known prior to observation. In addition, information about incidence angles is required, as the backscattering cross-section of a target depends on its incidence angle. Particularly in X-band observation, the antenna roll angle is variable and is set at a value that will maximize the antenna gain over the target observation area. For some targets, the observation direction (direction of emitted radio waves) is another important parameter. Further, in mountainous areas, the flight altitude of the aircraft becomes substantially lower due to the effect of ground height. In such cases the slant range shifts from the correct value and the target may go out of the observation range. We must take these factors into account when determining observation parameters. In addition, when measuring steep mountainous areas, we must determine the incidence angle so as not to cause foreshortening or produce shadows on slopes. In this manner, a flight plan is designed to cover about ten observation paths per day, to most efficiently execute the required observation. The aircraft on which the airborne SAR is installed is capable of continuous flight at an altitude of 12,000 m at about 220 m/s for about four hours. This translates into a distance of more than 3,000 km, which would appear largely sufficient in terms of observation. In fact, the net observation time is approximately half of the above-mentioned maximum flight time, as the observations require a certain lead time for stabilization of airplane attitude (including drift angle) before entering the respective flight path, and the aircraft needs time to ascend, descend, move between flight paths, and turn around.

4.2 Operation

When a proper observation plan is made, the starting observation position, the observation mode, the observation distance, and the parameter settings can be saved in a parameter file before the flight of experiment. When starting actual observations, we read out this parameter file to establish the observation mode, saving time in preparations and preventing erroneous parameter settings. On the day of observation, we first check the weather conditions and the flight course and activate the INS and GPS before takeoff. Nitrogen is filled in the X-band wave guide under pressure to prevent discharge prior to takeoff. When approaching the observation site, the operator begins observation following the steps listed on Table 3, based mainly on the information provided by the pilot. When the

aircraft has arrived at the point at which straight flight will begin, the pilot stabilizes the drift angle so as to maintain the flight course and notifies the operator of the timing for commencement of observations. The operator for X-band observation then makes temporary settings for antenna roll angle and yaw angle to correct for drift angle. The operator is then notified of the start timing and makes the appropriate settings for the observation parameters. We set aside about 10 seconds for averaging of the aircraft altitude and drift angle. When the parameter setting have been completed, the SAR system controls the recorder and, when the tape is running smoothly, begins observations after three seconds of noise observation and 15 seconds of receiver calibration. Table 3 shows the relevant timetable (indicating only the essential items for such settings). Operators are absorbed in final verification of observation parameters and hardware conditions during observations.

Table 3 *Operation flow (per observation path)*

Relative time (sec) (observation start time = 0)	Message	Messenger
-420	Approximately three minutes to the course of straight flight	Pilot
-380	Set temperature	X-operator to L-operator
	check wave guide pressure	
-240	Begin straight flight	Pilot
-230	Read observation parameters,	X-operator to L-operator
	check parameters	X-, L-operators
-160	Get flight information and temporary setting	X-operator
-120	Report drift angle	Pilot
-60	Operation start point	Pilot
	About 10 seconds after	
-50	Get flight information and parameter setting	X-operator to L-operato
-25	Prepare to begin observation	
-18	Acquire noise data	
-15	Calibration	
0	Begin observation (transmit radio waves)	
	End observation point	Pilot
	End Cal. and Noise notification; move to next path	X-, L-operators X-operator to pilot

5 Data Processing Subsystem

The higher the horizontal resolution becomes, the greater the amount of data acquired in SAR observation. Accordingly, data readout and data processing will take longer. Fortunately, the data processing speed of processors and the capacity of storage media have improved remarkably in recent years. We have continually upgraded the SAR data processing system in step with such improvements. Described below is the system status as of the end of 2001.

5.1 Hardware

Fig.7 presents configuration of the SAR processing system.

In this figure, SAR data processing computer and SAR application processing computer are separated only for convenience; they do not each feature customized programs. Thus either computer may be used as backup for the other, and their connections are configured to enable both primary and backup functions. Raw data is read out to a D1 tape device connected to the primary calculator via SCSI interface and is subject to Level-0 processing to arrive at a predetermined data format. Since approximately five minutes of observation in the X-band provides 19 GB of data (at maximum), a 180-GB HDD can only serve as temporary storage. Thus we save data that has been subject to Level-0 processing to a 180-GB DTF tape. This basic data-processing system is duplicated; thus, parallel processing is possible.

After producing the Level-0 data, we check the hardware and conduct browse processing (10 m per pixel) for catalog preparation purposes. This processing is carried out on data acquired from all flight paths, and obtained data will be added to the catalog information. Later, SAR images are processed. The image size is 5 km × 5 km, and approximately 1.5 hours is required for data processing of one scene of single polarimetric data. Data that has gone through basic pro-

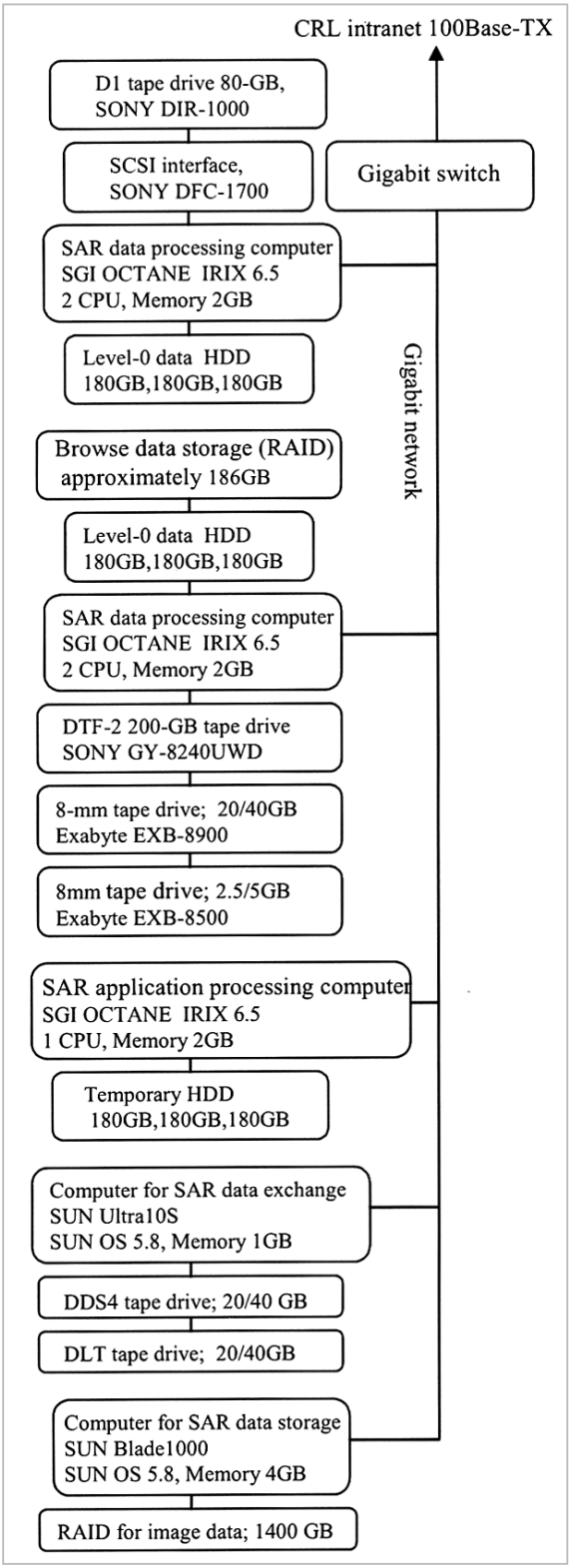

Fig.7 *Confinguration of SAR processing system*

cessing such as single-look slant-range complex (SSC) data and multi-look ground-range amplitude (MGA) data is saved to a hard disk in the file server and sent through the network, at which point it is subject to higher-level data processing, as necessary.

5.2 Software for data processing

SAR software can be divided into three categories, depending on function, as follows:
(1) Level-0 data production;
(2) Image production; and
(3) Distributed data production

The contents of each process are described below.

(1) Level-0 data production

Raw data recorded to the data tape during the experiment flight is read out for the production of Level-0 data. More specifically, the main process consists of the separation of received signals based on the types of polarized waves and observation modes involved (i.e., calibration, noise data, or actual observations). At the same time, a file is made of flight information for each data frame; these files will be required when performing motion compensation and when referring to radar settings during observation.

(2) Image production

The image production process is divided into the following four steps, which feature different data formats for output. Appendix-1 lists the formats for individual products, in addition to other relevant items.

(a) Single-look slant-range complex image production

In this step, as the central element of image reproduction, range compression and azimuth compression are performed, with correction of radar parameters and motion compensation of the aircraft based on the received signals. The received signals are visualized in this process. This step will be explained in more detail later.

(b) Multi-look ground-range amplitude image production

The power of SSC data is calculated and subjected to multi-look processing (4-look for Pi-SAR) to perform conversion from slant-range data to ground-range data.

(c) Multi-look ground-range polarimetric image production

SSC data is converted into the Muller matrix and subject to multi-look processing. After calculation of the components in the complex scattering matrix, slant-range to ground-range conversion is performed.

(d) Interferometric processing

In this calculation, phase difference is derived from the phase difference obtained with the main and sub antennas by removing phase difference from a plane. Further, coherence between data sets is calculated to provide multi-look slant-range interferometric images and multi-look slant-range coherence images as output.

In addition, the "browse image production" process is performed to check observation conditions, confirm the observation range, and prepare catalog data. The size of browse image is 20 km long in the range direction and 50 km long in the azimuth direction with one pixel size being 10 m.

(3) Preparation of materials for users

In principle, the obtained data is compressed and recorded in CD-ROM and other media formats for easy distribution in this step. We have adopted JPL's SIR-C "SLC" quad-pol data method for compression. This method enables the compression of an original 2,048 MB of data [for 4 ch-SSC images (8 bytes × 4) for each 5 km × 5 km area] to 10 bytes per pixel, to fit on a 640 MB CD.

5.3 SSC Image Production

This section explains single-look slant-range complex image production, which represents the core of the actual reproduction process.

(1) Range compression

I and Q data saved in the recorder consists of power data sets containing information on phases that are separated by 90 degrees. This data is converted into complex numbers. We correct the DC bias (zero level adjustment) and gain for both the I and Q data sets in order to average fluctuations in the characteristics of A/D converters. Gain/phase changes in the receiver amplifiers and attenuators are also corrected. The data is then subject to the range compression described in Section **2.2**, in a matched-filter process. In fact, this represents a convolution calculation, using the range reference function in the given frequency region. With $S_{ref}(f\tau)$ representing the results of Fourier transform of the range reference function, $S_{rev}(f\tau)$ representing the Fourier transform of received waves, and $W(f\tau)$ representing the window function in the current frequency region,

$S_{rc}(f\tau) = W(f\tau)\, S_{rcv}(f\tau)\, S^{*}_{ref}(f\tau)$

where * represents the complex conjugate number.

The range compression signal is obtained by inverse Fourier transform of $S_{rc}(f\tau)$.

(2) Radiometric correction

In addition to corrections related to the receiver, the range-compressed signal undergoes transmitter level correction, antenna elevation correction, and attenuation correction (dependent on the propagation distance of the radio waves).

(3) Aircraft motion compensation

Motions in height and attitude of the cause shifting and phase rotation in slant-range pixels. Thus the influence of these motions should be removed prior to azimuth compression. If the motion-induced shifts in position of the transmission antenna [y: cross-track direction (+: left), z: vertical direction (+: upward)] relative to the reference course of the aircraft are expressed by $\Delta y_{trans}(y)$, $\Delta z_{trans}(y)$, and if similarly, those of the reception antenna are expressed by $\Delta y_{rcv}(y)$, $\Delta z_{rcv}(y)$, the look angle is $\theta(\tau)$, and the wavelength of the adopted microwave is λ, then the slant-range shift $\Delta r(t,\tau)$, and phase rotation $\Delta\phi(t,\tau)$ are expressed by:

$$\Delta r(t,\tau) = \left[\Delta y_{trans}(t) * \sin\theta(\tau) - \Delta z_{trans}(t) * \cos\theta(\tau)\right] + \left[\Delta y_{rcv}(t) * \sin\theta(\tau) - \Delta z_{rcv}(t) * \cos\theta(\tau)\right] \quad \Delta\phi(t,\tau) = \frac{2\pi}{\lambda}\Delta r(t,\tau)$$

Among these correction quantities, the positional information (derived by integrating the INS data that was recorded with the received signals) is embedded in the independent GPS positioning data. The attitude data is calculated by integrating the angular acceleration detected by a gyro installed in the

INS. Transmission pulses must be resampled with reference to this positional information. Thus, based on this aircraft attitude data, resampling is carried out in order to maintain phase information using a finite impulse response (FIR) filter with linear phase characteristics. The filter length and sampling interval are variable.

(4) Estimate of center Doppler frequency

The center Doppler frequency is easily estimated, provided that the information about aircraft attitude and speed are precisely known. However, in most cases, it is difficult to measure the aircraft attitude precisely. Therefore, the Pi-SAR processing system is using the positional information provided by the above-mentioned aircraft motion compensation, instead of estimating the center Doppler frequency.

Nevertheless, it is also possible to conduct correction using the estimated center Doppler frequency, as follows. First, the azimuth-line signal previously subject to range compression is converted into the Doppler frequency region to allow estimation of its power. We examine the correlation between the estimated power and round-trip azimuth antenna pattern corresponding to the Doppler frequency, and determine the frequency that shows the peak of such correlation. This frequency, however, will feature uncertainty equivalent to an integral multiple of the pulse-repetition frequency. This instability is corrected based on the center Doppler frequency provided by the aircraft attitude correction. This value is estimated in several different range positions and is calculated by least-square interpolation.

(5) Correction of range migration

Considering the airplane's trajectory relative to a point on the ground, we can express the slant-range distance by a quadratic equation that provides the shortest distance to the target, i.e., when it is located to the immediate left of the plane. As a preliminary process prior to azimuth compression, we have to correct the range distance (or arrange the distances in a different sequence) within the adopted bandwidth. This correction process is called "migration correction." We convert the time-axis data into frequency-axis data and calculate the movement at the same Doppler frequency so that all of the target information is arrayed in the azimuth line.

(6) Azimuth compression

This is a data processing operation by which the reference azimuth wave is created from the center Doppler frequency and average speed of the aircraft followed by correlation with signals that have experienced range migration. This process is also a correlation calculation in the adopted frequency region, as in the case of range compression. If $S_{ref\text{-}az}(f,\tau)$ is the Fourier transform of the reference azimuth wave, $S'_{rc}(f,\tau)$ is that of the signal subject to range migration and W (f) is the window function, then azimuth compression signal can be provided by inverse Fourier transform of a correlation calculation $S_{ac}(f,\tau) = W(f)\, S'_{rc}(f,\tau)\, S^*_{ref\text{-}az}(f,\tau)$ where * represents the complex conjugate number.

6 Evaluation of the Pi-SAR System

(1) Resolution

In general, the resolution of a synthetic aperture radar is expressed by $\Delta r = c/2B$ in the slant-range direction, as mentioned earlier, where B is transmitter bandwidth. The azimuth resolution (single-look) is given by $\Delta Az = D/2$, where D is the real antenna aperture length (usually around 1.2 times the real antenna length).

The process used in general analysis is also used to perform multi-look so that the azimuth-direction resolution may become as high as the range-direction resolution and thereby reduce speckle noise.

In X-band resolution, when the transmitter bandwidth is 100 MHz and the antenna length is 1.05 m, then $\Delta r = 1.5$ m and $\Delta Az = 0.63$ m, while in L-band resolution, when the transmitter bandwidth is 50 MHz and the antenna length is 1.55 m, $\Delta r = 3.0$ m and $\Delta Az = 0.93$ m are expected. When evaluating the resolution of SAR, we need a point target in a location where the background scattering level is low.

For this purpose, CRL conducted a calibration experiment by deploying corner reflectors at Tottori dune. Fig.8 shows the obtained calibration data. This figure indicates that the range resolution is approximately 1.5 m and that azimuth resolution is 0.83 m in X-band resolution, while the range resolution is approximately 2.9 m and azimuth resolution is

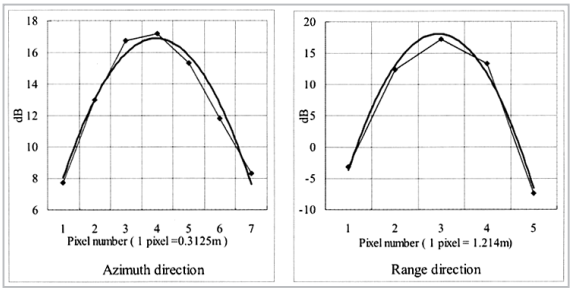

Fig.8 *Response from CR (X-band)*

1.2 m in L-band resolution; these results are in near agreement with the design specifications.

(2) Minimum receiving sensitivity

The SAR system conducts internal calibration and noise data before and after each observation. The minimum receiving sensitivity can be estimated from this data. The level diagram indicates that the noise level, which is measured based on the power at the output terminal of the receiver, lies between -77 dB and -87 dB. Fig.9 presents sample calibration data. This indicates that the input level is almost linear in the region from approximately -88 dB. Thus the minimum receiving sensitivity is nearly equivalent to the noise level (-87 dB), which is well beyond the specified level of -80 dB or less.

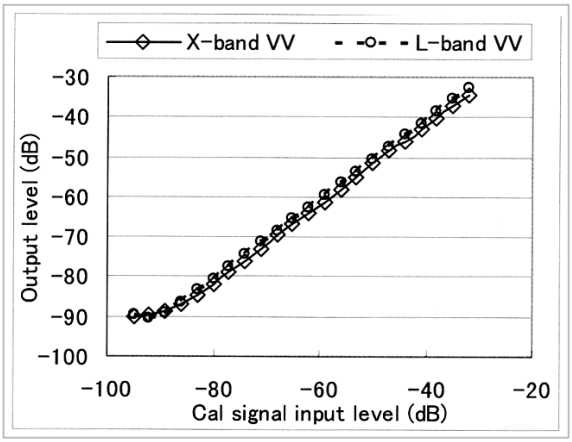

Fig.9 *Input/output characteristics of the receiver*

(3) Ground projection accuracy

In Pi-SAR data processing for data projection in the ground-range direction, projection on the ground surface is carried out based on the slant-range information about flight height and incidence angle at each observation site, assuming that the ground elevation is uniform in the area under observation. In order to examine the pixel position in the ground-range direction, we deployed several corner reflectors over about 10 km in the range direction in Ohgata village in Akita prefecture. We then compared the determined positions of these reflectors with the position data obtained by GPS. We found that the ground-projection accuracy declined in proportion to the magnitude of errors in flight height. When ground projection was carried out using the GPS system, the altitude error resulted in poor projection accuracy. However, Pi-SAR can estimate the altitude of the aircraft provided by interferometric processing. We found that ground projection based on this estimated height information would provide positioning accuracy as high as approximately one pixel.

In other words, when the ground height changes within the produced image, a ground projection error occurs from elevation change, unless the ground height data for each pixel position is taken [7].

(4) Interferometry

The error of interferometry is estimated by equation (1), in which the altitude error is 3.2 m where a phase-measurement error is 5 degrees at an altitude of 12,000 m and at an incidence angle of 45 degrees. In order to evaluate the accuracy of altitude data in real measurements, we conducted interferometry processing on the observation data for Ohgata village, Akita prefecture, and calculated altitude for purposes of comparison. Ohgata village, which was built on reclaimed land, featured almost no variations in ground elevation. In addition, since the unit size of each paddy was very large (90 m × 150 m), much larger than Pi-SAR's minimum area of resolution,

we were able to gather a sufficient quantity of data samples from a single paddy. Then we calculated the average and standard deviation of the data for several measurement points

Table 4 *Mean height and S.D. by incidence angles in Ohgata village*

	Normal		Ave. 3x3 pixels	
Inc. Angle	Average	S.D.	Average	S.D.
25 deg.	7.94m	1.50	7.92m	0.56
30 deg.	8.27m	2.54	8.24m	0.90
35 deg.	6.20m	3.00	6.16m	1.12
40 deg.	5.66m	4.13	5.68m	1.14
45 deg.	6.78m	5.09	6.74m	1.35
50 deg.	7.96m	6.00	8.08m	1.57
54 deg.	5.42m	7.02	5.30m	1.98

featuring different incidence angles. The calculation results are listed in Table 4.

Note that at the time of interferometry processing 2×2 averaging was performed on both the azimuth and range directions, and pixel spacing was 2.5 m. Approximately 600 pixels were used in this statistical treatment. The obtained results show that shallow incidence angles result in higher sensitivity to phase change and thus produce less error, and that some averaging improves the ground height accuracy. The required accuracy can be obtained by averaging over $(5\,\mathrm{m})^2$ - $(10\,\mathrm{m})^2$.

(5) Polarimetry

Polarization is expressed by a scattering matrix composed of four complex numbers, as described earlier. It is necessary to measure as correctly as possible the absolute value of these elements, and the relation between elements. Thus external calibration, using known targets, becomes necessary. In general, we are required to estimate inter-channel imbalance (with respect to phase and power) as well as to calculate the absolute values of the respective channels using corner reflectors (CR), and active radar calibrators (ARC). In the case of Pi-SAR, we had conducted calibrations using CR and ARC installed in Tottori dune and on ice in Saroma Lake[8]. Gain imbalances in the X- and L-band systems has been made public in the form of calibration coefficients (see the handout CD of Pi-SAR data and the CRL Web page). The level of cross-talk in both the X- and L-band ones is so low that it may be ignored. Since a patch antenna is adopted in L-band observation, the antenna position does not change between different polarization waves. On the other hand, in X-band observation, antennas in different positions are used for each polarization wave and the roll angle is variable. Thus a correction related to antenna position becomes necessary to gain accurate phase information[9]. Furthermore, for precise polarimetric calibration, it would be helpful to conduct a calibration experiment in which we installed a number of such reference targets at different incidence angles in the imaging area of interest. Such an experiment, however, is not practical to perform. Van Zyl et al. conducted calibrations[10] for JPL's AIRSAR, using natural targets as well as artificial ones. However, it is difficult to find a natural scattering target in Japan that is uniform over a wide range; thus we have been developing an alternative method of calibration.

7 Summary

The observation result obtained until now shows that the development target was almost attained about the system by which the airborne synthetic aperture radar together developed by Communications Research Laboratory and National Space Development Agency of Japan includes a data-processing function. Calibration coefficients for the radar have also been clarified through experiments employing corner reflectors deployed at Tottori dune. As we have added a real time processor unit to the basic hardware system, it can now be adopted quickly and effectively—in the event of emergency, for example. The system has been upgraded, whenever necessary, to accommodate massive data processing tasks, and modifications of the software have thus reached a satisfactory stage.

The future challenges regarding hardware include an exploration of the possibilities of along-track interferometry and real-time

downlink of data. In order to use the obtained Pi-SAR and other observation data more effectively, we anticipate moving forward in collaboration with research institutions that are extensively involved in related applications. In addition, we have distributed CD-ROMs to potential users that contain Pi-SAR data for various areas such as forests, farms, and oceans. We expect that more and more researchers will become interested in the Pi-SAR program and that synthetic aperture radar will be subject to further and more extensive investigation in the future.

Appendix-1. Formats of the products

(1) Data products

Single-look Slant-range Complex: SSC

Processing

Range compression

Single-look azimuth compression

4-byte + 4-byte complex

SSC					
	Bandwidth	Resolution (m)		Pixel (m)	
		Az [1]	Sr [1]	Az [2]	Sr
X-SAR	100MHz	0.375	1.5	0.261	1.214
	50MHz	0.375	3.0	0.261	2.428
L-SAR	50MHz	0.750	3.0	0.522	2.428

[1:] Theoretical value without any window function

[2:] Nominal value (depends on airplane speed and PRF)

Multi-look Ground-range Amplitude: MGA

Processing

Multi-look processing of SSC data

Slant-range to ground-range conversion

Calculation to Amplitude

2-byte integer

Multi-look Ground-range Polarimetric: MGP

Processing

Calculate complex scattering matrix from SSC data

Transform to Muller matrix, multi-look processing and transform to scattering matrix

Slant-range to ground-range conversion

4-byte + 4-byte complex

MGA/MGP						
	Bandwidth	Look number	Resolution (m)		Pixel (m)	
			Az [1]	Gr [1 2]	Az	Gr
X-SAR	100MHz	4look	1.5	1.6-17.2	1.25	1.25
	50MHz	8look	3.0	3.2-34.4	2.50	2.50
L-SAR	50MHz	4look	3.0	3.5-8.8	2.50	2.50

[1:] Theoretical value without any window function

[2:] Incidence angle of 20 to 60 degrees

Browse image

1-byte integer

Image swath 50 km (azimuth)×20 km (range)

Resolution of about 10 m (range)×10 m (azimuth)

(2) Data-file structure

The decompressed file has no header or the like. Instead, data sets are repeated as many times as there are azimuth-direction data points along a single azimuth line.

Coordinates in the image

Azimuth direction			
(1 , 1)	·····	(N_x , 1)	
:		:	Range direction
(1 , N_y)	·····	(N_x , N_y)	

N_x: Data-point number in the azimuth direction
N_y: Data-point number in the range direction

(a) Data arrangement in each file of decompressed MGP data

Re (1 , 1)	Im (1 , 1)	·····	Re (N_x , 1)	Im (N_x , 1)
:	:		:	:
Re (1 , N_y)	Im (1 , N_y)	·····	Re (N_x , N_y)	Im (N_x , N_y)
4-byte real	4-byte real			

(b) Data arrangement in each file of decompressed power (VV-mode) data

Amp (1 , 1)	·····	Amp (N_x , 1)
:		:
Amp (1 , N_y)	·····	Amp (N_x , N_y)
4-byte real		

Decompressed data is of the following size:

(a) nnnn* (8-byte complex number data*mmmm)*4 polarized waves
(b) nnnn* (4-byte real number data*mmmm)

If nnnn = 4,000 and mmmm = 3,000, then the sizes are given by:
(a)4,000* (8*3,000)*4 = 384 MB, (b)4,000*4*3,000 = 48 MB.

(3) Reference information

The distributed data includes a reference information file that has "_a" at the end of the file name. This includes observation information about altitude and airplane speed, latitude/longitude of the processing site, incidence angle, pixel number, pixel size, and window function processing. You can refer to this information file together with the JPEG data in this document. It may prove helpful for reference when analyzing reproduced images.

References

1 T.Kozu, et al., "Researh on Compact and High-performance Airborne Imaging Radar for Wide-area Monitoring of Oil Pollution ", Environment Preservation Reports, pp.84-1 to 84-12,1989.

2 F.T.Ulaby, R.K.Moore and A.K.Fung, "Microwave Remote Sensing active and passive ", Artech House,Inc. MA,Vol.2,1982.

3 Curlander,J.C. and R. MacDonough, "Synthetic Aperture Radar: Systems and Signal Processing ", John Willy & Sons, New York,1991.

4 Allen, C.T., "Interferometric Synthetic Aperture Radar ", IEEE Newsletter, Sep. 1995.

5 Development of Three-dimensional Airborne SAR at CRL, Tech.Rep.IEICE, SEAN95-99,33-38,1995.

6 T. Kobayashi, et al., "Airborne Dual-Frequency Polarimetric and Interferometric SAR", IEICE Trans. Commun., Vol.E83-B, No.9, pp.1945-1954, 2000.

7 T.Umehara, et al. , "Accuracy validation of ground projection Pi-SAR images ", RSSJ, No31pp.267-268,2001.

8 M. Satake, et al., "Calibration of an X-band Airborne Synthetic Aperture Radar with Active Radar Calibrators and Corner Reflectors ", CEOS 1999 SAR Workshop, Toulouse, France, 1999.

9 M. Satake, et al., "Development and Experiment of Polarization Selective Corner Reflectors for Polarimatric SAR Calibration ", 2001 CEOS SAR Workshop, Tokyo, Japan, 2001.

10 J.J.van Zyl, "Calibration of polarimetric radar images using only image parameters and trihedral corner reflectors ", IEEE Tans. Geoscience Remote Sensing, Vol.28, No3, pp.337-348,1990.

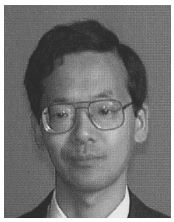

UMEHARA Toshihiko

Senior Researcher, Environment Information Technology Group, Applied Research and Standards Division

Global Environment Remote Sensing

E-mail; umehara@crl.go.jp

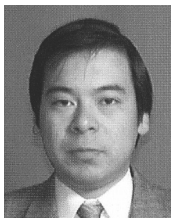

***KOBAYASHI Tatsuharu**, Dr. Sci.*

Senior Researcher, Environment Information Technology Group, Applied Research and Standards Division

Remote Sensing by Microwave

E-mail; tkoba@crl.go.jp

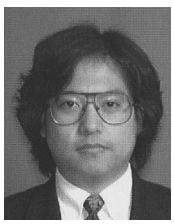

NADAI Akitsugu

Senior Researcher, Environment Information Technology Group, Applied Research and Standards Division

Physical Oceanography, Ocean Remote Sensing

E-mail; nandai@crl.go.jp

***MASUKO Harunobu**, Dr. Sci.*

Executive Director, Applied Research and Standards Division

Microwave Remote Sensing

E-mail; masuko@crl.go.jp

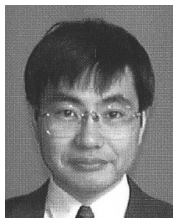

***URATSUKA Seiho**, Dr. Eng.*

Leader, Environment Information Technology Group, Applied Research and Standards Division

Microwave Remote Sensing

E-mail; pata@crl.go.jp

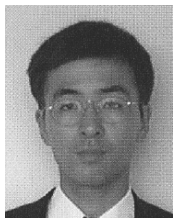

SATAKE Makoto

Senior Researcher, Environment Information Technology Group, Applied Research and Standards Division

Microwave Remote Sensing

E-mail; satake@crl.go.jp

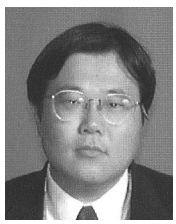

MAENO Hideo

Senior Researcher, Environment Information Technology Group, Applied Research and Standards Division

Pi-SAR, Remote Sensing

E-mail; maeno@crl.go.jp

***SHIMADA Masanobu**, Ph. D.*

Senior Engineer, Earth Observation Research Center, National Space Development Agency of Japan

Global Environment Remote Sensing

E-mail; shimada@eorc. nasda.go.jp